EFFECT OF CURVATURE ON THE BACKSCATTERING FROM LEAVES

K. Sarabandi, T. B. A. Senior and F. T. Ulaby

Radiation Laboratory
The University of Michigan
Department of Electrical Engineering and Computer Science
Ann Arbor, MI 48109-2122

Abstract -- Using a model previously developed for the backscattering cross section of a planar leaf at X-band frequencies and above, the effect of leaf curvature is examined. For normal incidence on a rectangular section of a leaf curved in one and two dimensions, an integral expression for the backscattered field is evaluated numerically and by a stationary phase approximation, leading to a simple analytical expression for the cross section reduction produced by the curvature. Numerical results based on the two methods are virtually identical, and in excellent agreement with measured data for rectangular sections of coleus leaves applied to the surfaces of styrofoam cylinders and spheres of different radii.

1. Introduction

Leaves are an obvious part of any vegetation canopy. They can vary in size, shape, orientation, moisture content, etc., and if we are to model the backscattering from a canopy, it is necessary to compute the backscattering from a single leaf [1], [2]. In a recent study [3] it was shown that for a typical planar leaf at X-band frequencies and above, a resistive sheet model in conjunction with the physical optics approximation accurately predicts the backscattering cross section at almost all angles

This work was supported by the National Aeronautics and Space Administration under Contract NAG5-480.

of incidence. The (complex) resistivity of the sheet is a function of the gravimetric moisture content Mg of the leaf, and for all moisture contents, the accuracy of the resulting prediction is adequate for most practical purposes.

In their natural state leaves are not generally planar, and any curvature may reduce their backscattering cross sections. To explore this effect, measurements have been carried out using a rectangular portion of a coleus leaf attached to the surfaces of styrofoam cylinders and spheres of different radii. For a wide range of curvatures, the reduction in the backscattering cross section at X band is accurately predicted by the physical optics approximation, and the results of a numerical evaluation of the physical optics integral are almost identical to a Fresnel integral expression derived from a stationary phase evaluation.

2. Leaf Model

A leaf can be regarded as a thin, non-magnetic lossy dielectric layer, and an effective model for such a layer is an infinitesimally thin resistive sheet. The sheet is simply an electric current sheet characterized by a (complex) resistivity R where

$$R = \frac{iZ}{k\tau(\varepsilon - 1)}. \qquad (1)$$

Here, k and Z are the propagation constant and intrinsic impedance respectively of free space, τ is the layer thickness, ε is the complex dielectric constant of the material, and a time factor $e^{-i\omega t}$ has been assumed and suppressed.

The dielectric constant $\varepsilon = \varepsilon' + i\varepsilon''$ of a leaf is primarily determined by its

gravimetric moisture content Mg, and can be found using a Debye-Cole dual-dispersion dielectric model [4]. The model predicts ε' and ε'' in terms of the frequency, temperature and Mg, and approximate empirical expressions valid at X-band and room temperatures are available [3]. The accuracy is within ±20%. The thickness τ of a leaf also depends on its moisture content and decreases with decreasing Mg. In reality, however, the thickness generally decreases from base to tip and may vary by as much as 50 percent over the surface. For a class of coleus leaves, an approximate expression for the average thickness in terms of Mg was given in [3], but for the coleus leaves used in the present study the thickness was measured at several points using calipers, and the averages determined. It is worth noting that the resulting resistivity of the leaf was in good agreement with the value of R measured using a leaf section placed in a waveguide.

At X-band frequencies and above the physical optics approximation applied to the resistive sheet model provides an accurate estimate of the backscattering cross section of a planar leaf for all moisture contents and most angles of incidence. For a sheet lying in the plane $\xi = 0$ of a Cartesian coordinate system (ξ, η, ζ) and illuminated by a plane electromagnetic wave having

$$\bar{E}^i = (\hat{\xi} \sin\alpha \sin\phi + \hat{\eta} \sin\alpha \cos\phi + \hat{\zeta}\cos\alpha)\, e^{-ik(\xi\cos\phi - \eta\sin\phi)} \qquad (2)$$

(see Figure 1), the induced electric current is

$$\bar{J} = 2Y \{\hat{\eta} \sin\alpha\, \Gamma_H(\phi) + \hat{\zeta} \cos\alpha \cos\phi\, \Gamma_E(\phi)\}\, e^{ik\eta\sin\phi} \qquad (3)$$

where [3]

$$\Gamma_H(\phi) = \left(1 + \frac{2R}{Z}\sec\phi\right)^{-1},$$

$$\Gamma_E(\phi) = \left(1 + \frac{2R}{Z}\cos\phi\right)^{-1}.$$

Γ_H and $-\Gamma_E$ respectively are the plane wave reflection coefficients for H polarization ($\alpha = \pi/2$) when the magnetic vector is perpendicular to the plane of incidence and for E polarization ($\alpha = 0$) when the electric vector is similarly inclined. Since R = 0 corresponds to perfect conductivity, Γ_H and Γ_E show how the current differs from the current $\bar{J}_{pc}$ supported by a perfectly conducting surface. Indeed,

$$\bar{J} = \bar{J}_{pc} \cdot \hat{\eta}\,\Gamma_H(\phi) + \bar{J}_{pc} \cdot \hat{\zeta}\,\Gamma_E(\phi) \qquad (4)$$

where $\hat{\eta}$ and $\hat{\zeta}$ are unit tangent vectors in and perpendicular to the plane of incidence respectively.

3. One Dimensional Curvature

In the Appendix expressions are derived for the backscattering cross section of a rectangular resistive plate of dimensions a, b as a function of the angle of incidence, and we now examine the effect of giving the plate a constant radius of curvature ρ in a principal plane. As a result of the bending, the plate conforms to a portion of the surface of a right circular cylinder of radius ρ as shown in Figure 2.

If the flat plate has length a in the z direction and width b in the y direction, then $b = 2\rho\phi_0$. The illuminating field is a plane wave propagating in the negative x direction with

$$\bar{E}^i = (\hat{y}\sin\alpha + \hat{z}\cos\alpha)\, e^{-ik(x-\rho)} \tag{5}$$

and in the backscattering direction the far field expression for the Hertz vector $\bar{\pi}$ is

$$\bar{\pi}(\bar{x}) = \frac{e^{ikx}}{kx}\,\frac{iZ}{4\pi}\,a\rho \int_{\theta-\phi_o}^{\theta+\phi_o} \bar{J}(\phi')\, e^{ik\rho(1-\cos\phi')}\, d\phi'$$

where the phase origin has been chosen at the front of the cylinder. To ensure that no portion of the outer surface of the plate is shadowed, it is necessary that $|\theta| \le \frac{\pi}{2} - \phi_o$.

The resistive sheet current $\bar{J}$ is given by (3) with the identification

$$\phi = \phi', \quad \hat{\eta} = -\hat{x}\sin\phi' + \hat{y}\cos\phi', \quad \hat{\zeta} = \hat{z}.$$

Recognizing that the exponent in (5) is simply the incident field phase at the surface,

$$\bar{J}(\phi') = 2Y\left\{(-\hat{x}\sin\phi' + \hat{y}\cos\phi')\sin\alpha\,\Gamma_H(\phi') + \hat{z}\cos\alpha\cos\phi'\,\Gamma_E(\phi')\right\} e^{ik\rho(1-\cos\phi')},$$

and hence

$$\bar{\pi}(\bar{x}) = \frac{e^{ikx}}{kx}\,\frac{ia\rho}{2\pi} \int_{\theta-\phi_o}^{\theta+\phi_o} \left\{(-\hat{x}\sin\phi' + \hat{y}\cos\phi')\sin\alpha\,\Gamma_H(\phi') + \hat{z}\cos\alpha\cos\phi'\,\Gamma_E(\phi')\right\} e^{2ik\rho(1-\cos\phi')}\, d\phi'.$$

The resulting backscattered far field amplitude is

$$\bar{S} = \frac{ik^2 a\rho}{2\pi} \int_{\theta-\phi_o}^{\theta+\phi_o} \left\{\hat{y}\sin\alpha\,\Gamma_H(\phi') + \hat{z}\cos\alpha\,\Gamma_E(\phi')\right\} \cos\phi'\, e^{2ik\rho(1-\cos\phi')}\, d\phi' \tag{6}$$

in terms of which

$$\sigma = \frac{\lambda^2}{\pi} \left| (\hat{y} \sin\alpha + \hat{z} \cos\alpha) \cdot \bar{S} \right|^2, \tag{7}$$

$$\sigma_{cross} = \frac{\lambda^2}{\pi} \left| (\hat{y} \cos\alpha - \hat{z} \sin\alpha) \cdot \bar{S} \right|^2. \tag{8}$$

Two methods were employed to evaluate the integral expression (6) for $\bar{S}$. In the first, the arc $\theta - \phi_o < \phi' < \theta + \phi_o$ was subdivided into 2M segments and each replaced by a planar strip of width $\Delta = \rho\phi_o/M$ centered at $\phi' = \phi'_m$, m = 1, 2, ..., M, and tangential to the cylinder. From the formula (A.3) for the backscattered far field amplitude of an inclined plate, we then have

$$\bar{S} = \frac{ik^2 a\Delta}{2\pi} \sum_{m=1}^{2M} \{\hat{y} \sin\alpha\, \Gamma_H(\phi'_m) + \hat{z} \cos\alpha\, \Gamma_E(\phi'_m)\} \cos\phi'_m\, e^{2ik\rho(1 - \cos\phi'_m)} \frac{\sin U'}{U'} \tag{9}$$

with $U' = k\Delta\sin\phi'_m$. The summation was carried out numerically, and a comparison with data obtained from a moment method solution of the integral equation for a curved resistive strip is given in Section 5.

The second method is entirely analytical and is based on the stationary phase (SP) approximation. The SP point of the integral in (6) is $\phi' = 0$ and on the assumption that $k\rho >> 1$, with $\theta < \phi_o$ so that the SP point lies within the range of integration,

$$\bar{S} = \frac{ika}{2\pi}\sqrt{k\rho}\left\{\hat{y}\sin\alpha\,\Gamma_H(0) + \hat{z}\cos\alpha\,\Gamma_E(0)\right\}\left\{\mathcal{F}\left[\sqrt{k\rho}\,(\phi_o+\theta)\right] + \mathcal{F}\left[\sqrt{k\rho}\,(\phi_o-\theta)\right]\right\}$$

where

$$\mathcal{F}(\tau) = \int_0^\tau e^{iu^2}\,du \tag{10}$$

is the finite range Fresnel integral. We remark that for $|\tau| << 1$

$$\mathcal{F}(\tau) = \tau + O(\tau^3), \tag{11}$$

whereas for $|\tau| >> 1$

$$\mathcal{F}(\tau) \sim \frac{1}{2}\sqrt{\pi}\,e^{i\pi/4}. \tag{12}$$

Since $\Gamma_E(0) = \Gamma_H(0)$ it now follows that

$$\bar{S} = \frac{ika}{2\pi}\sqrt{k\rho}\,(\hat{y}\sin\alpha + \hat{z}\cos\alpha)\,\Gamma_H(0)\left\{\mathcal{F}\left[\sqrt{k\rho}\,(\phi_o+\theta)\right] + \mathcal{F}\left[\sqrt{k\rho}\,(\phi_o-\theta)\right]\right\} \tag{13}$$

showing that to this approximation there is no depolarization in the backscattering direction.

It is instructive to examine separately the special case of symmetric (normal) incidence when $\theta = 0$. The argument of the Fresnel integrals in (13) is then $b/2\sqrt{k/\rho}$, and if $\rho >> kb^2/4$, the approximation (11) implies

$$\bar{S} = \frac{ik^2ab}{2\pi}(\hat{y}\sin\alpha + \hat{z}\cos\alpha)\,\Gamma_H(0), \tag{14}$$

in agreement with the known expression for the backscattered far field amplitude of a planar resistive plate at normal incidence. On the other hand, if $\rho << kb^2/4$, (12) gives

$$\overline{S} = -\frac{ka}{2}\sqrt{\frac{k\rho}{\pi}}\,(\hat{y}\sin\alpha + \hat{z}\cos\alpha)\,\Gamma_H(0)\,e^{-i\frac{\pi}{4}}$$

which is the result for a resistive circular cylinder of radius ρ and length a. For intermediate values of ρ the Fresnel integral must be retained, and when the far field amplitude is normalized to the flat plate expression (14), denoted by the affix fp,

$$\frac{S}{S^{fp}} = \frac{1}{\gamma}\mathcal{F}(\gamma) \qquad (15)$$

independent of the resistivity, where

$$\gamma = \frac{b}{2}\sqrt{\frac{k}{\rho}}\,. \qquad (16)$$

Calculations based on the formulas (9), (13) and (15) are compared with numerical results obtained using the moment method and with measured data in Section 5.

4. Two Dimensional Curvature

We now consider the effect of giving the plate the same curvature in both principal planes, so that the plate conforms to a portion of a spherical surface of radius r. For simplicity the analysis is carried out for a plane wave incident symmetrically, and the geometry is then as shown in Figure 3.

In terms of the spherical polar coordinates r, θ', φ' such that $x = r\sin\theta'\cos\phi'$, $y = r\sin\theta'\sin\phi'$ and $z = r\cos\theta'$, the plate occupies the surface region $\frac{\pi}{2} - \theta_o < \theta' < \frac{\pi}{2} + \theta_o$, $-f(\theta') < \phi' < f(\theta')$ where $\theta_o = b/(2r)$ and $f(\theta') = a/(2r\sin\theta')$. The incident electric field is the

same as that in Section 3, and for a perfectly conducting plate the physical optics expression for the induced electric current at a point θ', ϕ' on the surface is

$$\bar{J}_{pc} = 2Y\left\{\sin\alpha \sin\theta'(-\hat{x} \sin\phi' + \hat{y} \cos\phi') + \cos\alpha(-\hat{x} \cos\theta' + \hat{z} \sin\theta'\cos\phi')\right\} e^{ikr(1 - \sin\theta'\cos\phi')}.$$

Unit vectors tangential to the surface and parallel and perpendicular respectively to the plane of incidence are

$$\hat{\eta}_1 = Q\{-\hat{x}(1 - \sin^2\theta' \cos^2\phi') + \hat{y}(\sin\theta' \sin\phi' + \hat{z} \cos\theta') \sin\theta' \cos\phi'\},$$

$$\hat{\zeta}_1 = Q(-\hat{y} \cos\theta' + \hat{z} \sin\theta' \sin\phi')$$

where

$$Q = (1 - \sin^2\theta' \cos^2\phi')^{-1/2},$$

and in terms of $\hat{\eta}_1$ and $\hat{\zeta}_1$ the perfectly conducting plate current is

$$\bar{J}_{pc} = 2Y\{(\sin\alpha \sin\theta' \sin\phi' + \cos\alpha \cos\theta')\hat{\eta}_1 - \sin\theta' \cos\phi' (\sin\alpha \cos\theta'$$

$$- \cos\alpha \sin\theta' \sin\phi')\hat{\zeta}_1\} Q e^{ikr(1 - \sin\theta' \cos\phi')}$$

From (4) it now follows that for a resistive plate the current is

$$\bar{J} = 2Y\{(\sin\alpha \sin\theta' \sin\phi' + \cos\alpha \cos\theta')\Gamma_H(\phi)\hat{\eta}_1 - \sin\theta' \cos\phi' (\sin\alpha \cos\theta'$$

$$- \cos\alpha \sin\theta' \sin\phi')\Gamma_E(\phi)\hat{\zeta}_1\} Q e^{ikr(1 - \sin\theta' \cos\phi')} \qquad (17)$$

where the angle ϕ is such that

$$\cos\phi = \sin\theta' \cos\phi'.$$

In the backscattering direction the far field expression for the Hertz vector $\bar{\pi}$ is

$$\bar{\pi}(x) = \frac{e^{ikx}}{kx}\,\frac{iZr^2}{4\pi}\int_{\frac{\pi}{2}-\theta_o}^{\frac{\pi}{2}+\theta_o}\int_{-f(\theta')}^{f(\theta')} \bar{J}(\theta', \phi')\, e^{ikr(1\,-\,\sin\theta'\cos\phi')}\sin\theta'\, d\theta'\, d\phi',$$

and when the formula (17) for $\bar{J}$ is inserted, the backscattered far field amplitude for the curved resistive plate is found to be

$$\begin{aligned}\bar{S} = \frac{ik^2r^2}{2\pi}\int_{\frac{\pi}{2}-\theta_o}^{\frac{\pi}{2}+\theta_o}\int_{-f(\theta')}^{f(\theta')}\Big[&\sin\alpha\,\hat{y}\,\{\sin^2\theta'\sin^2\phi'\,\Gamma_H(\phi) + \cos^2\theta'\,\Gamma_E(\phi)\}\\ &+ \cos\alpha\,\hat{z}\,\{\sin^2\theta'\sin^2\phi'\,\Gamma_E(\phi) + \cos^2\theta'\,\Gamma_H(\phi)\}\\ &+ (\cos\alpha\,\hat{y} - \sin\alpha\,\hat{z})\sin\theta'\cos\theta'\sin\phi'\,\{\Gamma_E(\phi) - \Gamma_H(\phi)\}\Big]\\ &\cdot Q^2\sin^2\theta'\cos\phi'\, e^{2ikr(1\,-\,\sin\theta'\cos\phi')}d\theta'\, d\phi'. \qquad (18)\end{aligned}$$

The like- and cross-polarized backscattering cross sections can be computed by substituting (18) in (7) and (8), and depolarization occurs to the extent that Γ_H and Γ_E differ over those portions of the plate that contribute to the integral.

The expression for $\bar{S}$ was evaluated using methods similar to those employed in Section 3. The first method is numerical. By subdividing the θ' and ϕ' ranges into 2L and 2M increments respectively and treating each elementary patch as a rectangular flat plate centered at $\theta' = \theta'_\ell$, $\phi' = \phi'_m$ ($\ell = 1, 2, \ldots, L$; $m = 1, 2, \ldots, M$) with dimensions $\Delta_1 = r\Delta\theta'$, $\Delta_2 = r\sin\theta'_2\,\Delta\phi'$ where $\Delta\theta' = \theta_o/L$ and $\Delta\phi' = f(\theta')/M$, the result is

$$\bar{S} = \frac{ik^2}{2\pi}\sum_{\ell=1}^{2L}\sum_{m=1}^{2M}[\quad]\Delta_1\Delta_2\, Q^2\sin\theta'_\ell\cos\phi'_m\, e^{2ikr\,(1\,-\,\cos\theta'_\ell\cos\phi'_m)}\,\frac{\sin U_1}{U_1}\,\frac{\sin V_1}{V_1}. \qquad (19)$$

Here

$$U_1 = k\Delta_1 \cos\theta'_\ell \cos\phi'_m$$

$$V_1 = k\Delta_2 \sin\phi'_m$$

and [ ] denotes the terms in square brackets in (18).

The second method is based on the stationary phase approximation. The (double) SP point of the integrand in (18) is $\vartheta' = \pi/2$, $\phi' = 0$, and when all the non-exponential terms are removed from the integrand at this point, we have

$$\overline{S} = \frac{ik^2r^2}{2\pi}(\hat{y}\sin\alpha + \hat{z}\cos\alpha)\,\Gamma_H(0)\int_{\frac{\pi}{2}-\theta_o}^{\frac{\pi}{2}+\theta_o}\int_{-f(\theta')}^{f(\theta')} e^{2ikr(1\,-\,\sin\theta'\cos\phi')}\,d\theta'\,d\phi'$$

where we have used the fact that $\Gamma_E(0) = \Gamma_H(0)$. By expanding the exponent about the SP point and retaining only the quadratic terms, we then obtain

$$\overline{S} = \frac{2ikr}{\pi}(\hat{y}\sin\alpha + \hat{z}\cos\alpha)\,\Gamma_H(0)\,\mathcal{F}\left(\frac{a}{2}\sqrt{\frac{k}{r}}\right)\mathcal{F}\left(\frac{b}{2}\sqrt{\frac{k}{r}}\right), \tag{20}$$

showing that to this approximation there is no depolarization. The amplitude normalized to its flat plate value (14) is

$$\frac{S}{S^{fp}} = \frac{1}{\gamma_1}\mathcal{F}(\gamma_1)\cdot\frac{1}{\gamma_2}\mathcal{F}(\gamma_2) \tag{21}$$

independent of the resistivity where

$$\gamma_1 = \frac{a}{2}\sqrt{\frac{k}{r}}\,, \qquad \gamma_2 = \frac{b}{2}\sqrt{\frac{k}{r}}\,, \tag{22}$$

and the reduction in S_{fp} is simply the product of the factors appropriate to a one-dimensional curvature in each of the principal planes of the plate.

The extension to the case of a plane wave which is not incident symmetrically is trivial. If the plate is rotated through an angle θ about the y axis (see Figure 3) with $|\theta| \leq \pi/2 - \theta_o$ so that no part of the plate is shadowed, the far field amplitude corresponding to (20) is

$$\overline{S} = \frac{ikr}{\pi}(\hat{y}\sin\alpha + \hat{z}\cos\alpha)\,\Gamma_H(0)\,\mathcal{F}\left(\frac{a}{2}\sqrt{\frac{k}{r}}\right)\left\{\mathcal{F}\left[\frac{b}{2}\sqrt{\frac{k}{r}}\left(1+\frac{\theta}{\theta_o}\right)\right] + \mathcal{F}\left[\frac{b}{2}\sqrt{\frac{k}{r}}\left(1-\frac{\theta}{\theta_o}\right)\right]\right\} \qquad (23)$$

Here also the expression is a natural extension of the formula for a one-dimensional curvature.

5. Comparison with Experimental Data

To test the validity of the resistive sheet model and to explore the effect of leaf curvature, a series of measurements was carried out using rectangular leaf sections. Coleus leaves were chosen because they retain their moisture after being cut: at room temperature (23°C) the change in moisture content after 20 minutes was less than one percent. The scattering measurements were made at X-band in a small tapered anechoic chamber using an HP 8510A network analyzer. A schematic of the equipment is shown in Figure 4, and the general procedures employed are described

in [3]. The only significant improvements made to the original system were the introduction of an automatic target positioner to permit measurements at specified increments in angle, and the use of strings stretched between synchronously rotating stepper motors at the top and bottom of the chamber to facilitate the target support. Since a single linearly-polarized horn antenna was used to radiate and receive the signals, only the like-polarized backscattering cross section could be measured. A small metal sphere was employed for calibration.

Some results for a plane rectangular section of a leaf having $a = 1.33\lambda$ and $b = 2\lambda$ with $Mg = 0.7$ and $\tau = 0.5$ mm are shown in Figures 5 and 6. E polarization ($\alpha = 0$) was used in both cases. In Figure 5 the leaf was initially vertical ($\beta = 0$) and the data as a function of the rotation angle ϕ are in good agreement with the curve computed from (A.4). In Figure 6 the leaf was tilted back ($\beta = 8$ deg.) and a similar comparison with (A.8) is shown. For completeness, the cross polarized cross section computed using (A.9) is included in Figure 6.

With the confidence that physical optics in conjunction with the resistive sheet model is adequate for planar leaves, we now compared the predictions for curved leaves with moment method data and with experimental results. To check the accuracy of (9), the scattering was computed using a two-dimensional moment method code [5] for resistive strips extended to the three-dimensional case by assuming that the current is independent of z, and in Figure 7 the backscattering cross section computed using (9) is compared with moment method data for a curved leaf having radius of curvature

$\rho = 2\lambda$ and for a flat leaf ($\rho = \infty$). The overall agreement is good out to 50 and 70 degrees respectively, where the lower limit for the curved leaf corresponds to the onset of shadowing. In Figure 8 the Fresnel integral approximation (13) is compared with (9) for curved leaves having $\rho = 2\lambda$ and 3λ. The agreement is excellent as long as the stationary phase point is on the leaf, i.e. for $|\theta| < 28$ and 19 degrees respectively, but remains good for incidence angles out to about 45 degrees.

Experimental measurements were also performed. In the first experiment a rectangular leaf section of the same size as before was attached to the surface of a right circular cylinder of styrofoam and the normal incidence backscattering cross section was measured. Cylinders of six different radii were used and the cross sections were normalized to that of the planar leaf. The measured cross section reductions for E polarization are plotted as a function of ρ/λ in Figure 9 and compared with the curves computed using the numerical summation (9) and the stationary phase approximation (15). The agreement is excellent. As ρ/λ decreases from 11 to 1, γ increases from 0.76 to 3.14. Over the entire range, (9) and (15) yield virtually identical results, and (15) provides a simple and accurate expression for the cross section reduction.

For the case of a two dimensional curvature a similar experiment was performed in which a leaf section was mounted on the surface of a styrofoam sphere. Spheres of six different radii were used. To facilitate the mounting a naturally-curved leaf was chosen and cut to conform to the spherical region $\frac{\pi}{2} - \theta_o < \theta' < \frac{\pi}{2} + \theta_o$, $-\phi_o < \phi' < \phi_o$ where $\theta_o = b/(2r)$, $\phi_o = a(2r\sin\theta_o)$, with $a = 1.33\lambda$ and $b = 2\lambda$. The region is slightly

different from that specified in Section 5, and the leaf sections are no longer rectangular when flattened out, but calculations based on the summation (19) showed that the cross section reduction is the same for both. The measured data are compared with the numerical and analytical results (19) and (21) in Figure 10. The agreement is again excellent and confirms the validity of the simple formula (21) for curvature in two dimensions.

As evident from the preceding figures, curvature can have a significant effect on the backscattering cross section, and in a practical situation, it is important to know the frequency range where any curvature of a leaf must be taken into account. To this end, Figure 11 shows the normal incidence cross section reductions versus frequency for three leaf sections 6 cm on a side, curved in one dimension with radii 3, 6 and 12 cm. In all three cases $Mg = 0.7$, $\tau = 0.5$ mm and the frequency dependence implied by (1) and the Debye-Cole dielectric model was included. Once again (9) and (15) yield virtually identical results and if, for example, $\rho = 12$ cm, the curvature produces a significant effect only at C-band frequencies and above.

6. Conclusions

The resistive sheet model in conjunction with the physical optics approximation which was previously shown [3] to accurately predict the backscattering cross section of a planar leaf has now been extended to the case of a curved leaf. For a rectangular section of a leaf curved in one and two dimensions, the physical optics expression for the backscattered field as a function of the angle of incidence was evaluated

numerically and by a stationary phase approximation. The latter leads to simple analytical expressions for the cross section reduction produced by the curvature. Numerical results based on the two methods are virtually identical over a wide range of incidence angles and in excellent agreement with measured X-band data for rectangular sections of coleus leaves applied to surfaces of styrofoam cylinders and spheres of different radii. As a result of these comparisons, it is concluded that the curvature effect is accurately simulated by a multiplicative factor involving a Fresnel integral whose argument is a function of the relevant leaf dimension, the radius of curvature, the frequency, and the angle of incidence, but independent of the material properties of the leaf.

Appendix: Flat Plate Analysis

To illustrate the application of the formulas in Section 2, consider a rectangular resistive plate occupying the region $-\frac{a}{2} < \eta < \frac{a}{2}$, $-\frac{b}{2} < \zeta < \frac{b}{2}$ of the plane $\zeta = 0$ and illuminated by the plane wave (2) as shown in Figure 1. Since there is only an electric current induced in the plate, the scattered field can be attributed to an electric Hertz vector $\bar{\pi}$. In the backscattering direction the far field expression for $\bar{\pi}$ is

$$\bar{\pi}(\bar{r}) = \frac{e^{ikr}}{kr} \frac{iZ}{4\pi} \int\int \bar{J}(\eta, \zeta)\, e^{ik\eta \sin\phi}\, d\eta\, d\zeta$$

where the integration is over the illuminated surface of the plate, and if the physical optics approximation is employed, it is a trivial matter to determine $\bar{\pi}$. From (3)

$$\bar{\pi}(\bar{r}) = \frac{e^{ikr}}{kr} \frac{i}{2\pi} \int_{-a/2}^{a/2} \int_{-b/2}^{b/2} \left\{ \hat{\pi} \sin\alpha\, \Gamma_H(\phi) + \hat{\zeta} \cos\alpha \cos\phi\, \Gamma_E(\phi) \right\} e^{2ik\eta \sin\phi}\, d\eta\, d\zeta$$

$$= \frac{e^{ikr}}{kr} \frac{iab}{2\pi} \left\{ \hat{\eta} \sin\alpha\, \Gamma_H(\phi) + \hat{\zeta} \cos\alpha \cos\phi\, \Gamma_E(\phi) \right\} \frac{\sin U}{U} \qquad (A.1)$$

where

$$U = ka\sin\phi. \qquad (A.2)$$

The scattered field is

$$\bar{E}^s = \nabla \times \nabla \times \bar{\pi}$$

and in the far field

$$\bar{E}^s = \frac{e^{ikr}}{kr} \bar{S}$$

where the backscattered far field amplitude is

$$\bar{S} = \frac{ik^2ab}{2\pi}\left\{ (\hat{\xi}\sin\phi + \hat{\eta}\cos\phi)\sin\alpha\,\Gamma_H(\phi) + \hat{\zeta}\cos\alpha\,\Gamma_E(\phi)\right\}\cos\phi\,\frac{\sin U}{U}. \qquad (A.3)$$

In terms of $\bar{S}$ the like-polarized backscattering cross section is

$$\sigma = \frac{\lambda^2}{\pi}\left| (\hat{\xi}\sin\alpha\sin\phi + \hat{\eta}\sin\alpha\cos\phi + \hat{\zeta}\cos\alpha)\cdot\bar{S}\right|^2$$

and the cross-polarized cross section is

$$\sigma_{cross} = \frac{\lambda^2}{\pi}\left| (\hat{\xi}\cos\alpha\sin\phi + \hat{\eta}\cos\alpha\cos\phi - \hat{\zeta}\sin\alpha)\cdot\bar{S}\right|^2.$$

Thus

$$\sigma = 4\pi\left|\frac{ab}{\lambda}\{\sin^2\alpha\,\Gamma_H(\phi) + \cos^2\alpha\,\Gamma_E(\phi)\}\cos\phi\,\frac{\sin U}{U}\right|^2 \qquad (A.4)$$

and

$$\sigma_{cross} = 4\pi\left|\frac{ab}{\lambda}\sin\alpha\cos\alpha\{\Gamma_H(\phi) - \Gamma_E(\phi)\}\cos\phi\,\frac{\sin U}{U}\right|^2, \qquad (A.5)$$

and we observe that the cross-polarized return vanishes if at least one of $\sin\alpha$, $\cos\alpha$, or $\cos\phi$ is zero or $\Gamma_E(\phi) = \Gamma_H(\phi)$. This last condition is satisfied for a perfectly conducting plate.

The above example corresponds to the rotation of the direction of incidence in the $\xi\eta$ plane and is equivalent to the rotation of the plate through an angle ϕ about the ζ axis with the illumination fixed in space. A more general situation is that in which the plate is first tilted back through an angle β (see Figure A.1) prior to rotation. In terms of a rotated coordinate system ξ', η', ζ' where $\hat{\xi}' = \hat{\xi}\cos\beta + \hat{\zeta}\sin\beta$, $\hat{\eta}' = \hat{\eta}$, $\hat{\zeta}' = -\hat{\xi}\sin\beta + \hat{\zeta}\cos\beta$, the plate now occupies $-\frac{a}{2} < \eta' < \frac{a}{2}$, $-\frac{b}{2} < \zeta' \frac{b}{2}$, and the incident electric field is

$$\bar{E}^i = (\hat{\xi} \sin\alpha \sin\phi + \hat{\eta} \sin\alpha \cos\phi + \hat{\zeta} \cos\alpha)\, e^{-ik(\xi' \cos\beta \cos\phi - \eta' \sin\phi - \zeta' \sin\beta \cos\phi)}.$$

Since the unit vector normal to the plate is $\hat{\xi}'$, the physical optics expression for the current that would be induced if the plate were perfectly conducting is

$$\bar{J}_{pc} = 2Y \{-\hat{\xi} \cos\alpha \sin\beta \cos\phi + \hat{\eta} (\sin\alpha \cos\beta + \cos\alpha \sin\beta \sin\phi) + \hat{\zeta} \cos\alpha \cos\beta \cos\phi\}\, e^{ik(\eta' \sin\phi + \zeta' \sin\beta \cos\phi)},$$

which can be written as

$$\bar{J}_{pc} = 2Y \{(\sin\alpha \cos\beta \sin\phi + \cos\alpha \sin\beta)\hat{\eta}_1 + (\sin\alpha \sin\beta - \cos\alpha \cos\beta \sin\phi) \cdot \cos\beta \cos\phi\, \hat{\zeta}_1\} P\, e^{ik(\eta' \sin\phi + \zeta' \sin\beta \cos\phi)}$$

where

$$P = (1 - \cos^2\beta \cos^2\phi)^{-1/2}$$

and

$$\hat{\eta}_1 = P (-\hat{\xi} \sin^2\beta \cos\phi + \hat{\eta} \sin\phi + \hat{\zeta} \sin\beta \cos\beta \cos\phi)$$

$$\hat{\zeta}_1 = P (-\hat{\xi} \sin\beta \sin\phi + \hat{\eta} \sin\beta \cos\phi - \hat{\zeta} \cos\beta \sin\phi)$$

are, respectively, unit vectors in and perpendicular to the plane of incidence, lying in the plane of the plate. The current induced in the resistive plate is therefore

$$\bar{J} = 2Y \{(\sin\alpha \cos\beta \sin\phi + \cos\alpha \sin\beta)\, \Gamma_H(\phi_1)\hat{\eta}_1 + (\sin\alpha \sin\beta - \cos\alpha \cos\beta \sin\phi)$$

$$\cdot \cos\beta \cos\phi\, \Gamma_E(\phi_1)\hat{\zeta}_1\}\, P\, e^{ik(\eta' \sin\phi + \zeta' \sin\beta \cos\phi)} \qquad (A.6)$$

where ϕ_1 is the angle between the negative of the incident field direction and the normal to the plate, i.e. $\cos^{-1}(\cos\beta \cos\phi)$.

The Herz vector defining the backscattered field is

$$\bar{\pi}(\bar{r}) = \frac{e^{ikr}}{kr} \frac{iZ}{4\pi} \int_{-a/2}^{a/2} \int_{-b/2}^{b/2} \bar{J}(\eta', \zeta')\, e^{ik(\eta' \sin\phi + \zeta' \sin\beta \cos\phi)}\, d\eta'\, d\zeta',$$

and when the integration is performed we obtain

$$\bar{\pi}(\bar{r}) = \frac{e^{ikr}}{kr} \frac{iab}{2\pi} [(\sin\alpha \cos\beta \sin\phi + \cos\alpha \sin\beta)\, \Gamma_H(\phi_1)\, \hat{\pi}_1 + (\sin\alpha \sin\beta$$

$$- \cos\alpha \cos\beta \sin\phi) \cos\beta \cos\phi\, \Gamma_E(\phi_1)\hat{\zeta}_1] P \frac{\sin U}{U} \frac{\sin V}{V}$$

where U is given in (A.2) and

$$V = kb \sin\beta \cos\phi\,.$$

The resulting expression for the backscattered far field amplitude is

$$\bar{S} = \frac{ik^2ab}{2\pi}\,[\,(\hat{\xi}\sin\phi + \hat{\eta}\cos\phi)\,\{\sin\alpha\,[\cos^2\beta\sin^2\phi\,\Gamma_H(\phi_1) + \sin^2\beta\,\Gamma_E(\phi_1)\,]$$
$$+ \cos\alpha\sin\beta\cos\beta\sin\phi\,[\Gamma_H(\phi_1) - \Gamma_E(\phi_1)\,\}$$
$$+ \hat{\zeta}\,\{\cos\alpha\,[\sin^2\beta\,\Gamma_H(\phi_1) + \cos^2\beta\sin^2\phi\,\Gamma_E(\phi_1)\,]$$
$$+ \sin\alpha\sin\beta\cos\beta\sin\phi\,[\Gamma_H(\phi_1) - \Gamma_E(\phi_1)\,]\,\}\,]\,P^2\cos\beta\cos\phi\,\frac{\sin U}{U}\,\frac{\sin V}{V} \quad (A.7)$$

and we note that this reduces to (A.3) when $\beta = 0$. The backscattering cross sections are

$$\sigma = 4\pi\left|\,\frac{ab}{\lambda}\,\{(\sin\alpha\cos\beta\sin\phi + \cos\alpha\sin\beta)^2\Gamma_H(\phi_1) + (\sin\alpha\sin\beta\right.$$
$$\left. -\cos\alpha\cos\beta\sin\phi)^2\,\Gamma_E(\phi_1)\}\,P^2\cos\beta\cos\phi\,\frac{\sin U}{U}\,\frac{\sin V}{V}\,\right|^2 \quad (A.8)$$

and

$$\sigma_{cross} = 4\pi\left|\,\frac{ab}{\lambda}(\sin\alpha\cos\beta\sin\phi + \cos\alpha\sin\beta)\,(\sin\alpha\sin\beta - \cos\alpha\cos\beta\sin\phi)\right.$$
$$\left. \cdot\ \{\Gamma_H(\phi_1) - \Gamma_E(\phi_1)\}\,P^2\cos\beta\cos\phi\,\frac{\sin U}{U}\,\frac{\sin V}{V}\,\right|^2. \quad (A.9)$$

As required, these reduce to (A.4) and (A.5) when $\beta = 0$, and for all β the cross-polarized return vanishes for a perfectly conducting plate. A comparison with measured data for a leaf is given in Section 5.

Acknowledgement

This work was supported by NASA Grant NAG5-480, NASA/GSFC, Beltsville,

Figure Captions

Figure 1: Geometry for the scattering of a plane wave from a resistive sheet lying in the plane $\xi = 0$.

Figure 2: Geometry for the scattering of a plane wave from a resistive sheet which conforms to a portion of the surface of a right circular cylinder of radius ρ.

Figure 3: Geometry for the scattering of a plane wave from a resistive sheet which occupies a portion of the surface of a sphere of radius r at normal incidence.

Figure 4: Schematic of the RCS measurement system.

Figure 5: Comparison of the measured RCS with the theoretical expression (A.4) for a rectangular section (a = 4 cm, b = 6 cm) of a cut coleus leaf with Mg = 0.7 and τ = 0.5 mm for E-polarization ($\alpha = 0$), $\beta = 0$ and λ = 3 cm.

Figure 6: Comparison of the measured RCS (***) with the theoretical expression (A.8) (——) for the rectangular section of the coleus leaf with Mg = 0.7 and τ = 0.5 mm for E-polarization ($\alpha = 0$), β = 8 deg and λ = 3 cm. The theoretical cross polarized RCS (A.9) (xxx) is also shown.

Figure 7: RCS of a rectangular resistive sheet computed using the moment method (lines) and the numerical summation (9) (points) for $\rho = 2\lambda$ (---, xxx) and $\rho = \infty$ (——, 000). The size and resistivity of the sheet are the same as in Figure 5 with τ = 0.32 mm and λ = 3 cm.

Figure 8: RCS of a rectangular resistive sheet computed using the numerical summation (9) (lines) and the Fresnel integral approximation (13) (points) for $\rho = 2\lambda$ (---, xxx) and $\rho = 3\lambda$ (——, 000). The size and resistivity of the sheet are the same as in Figure 5 with τ = 0.32 mm and λ = 3 cm.

Figure 9: Comparison of the measured RCS (***) reduction at normal incidence with the numerical summation (19) (——) and the Fresnel integral approximation (15) (---) for a one dimensionally curved rectangular section of a coleus leaf versus radius of curvature (τ = 0.32 mm, λ = 3 cm).

Figure 10: Comparison of the measured RCS (***) reduction at normal incidence with the numerical summation (19) (——) and the Fresnel integral approximation (21) (---) for a spherically curved section of a coleus leaf versus radius of curvature (τ = 0.32 mm, λ = 3 cm).

Figure 11: Normal incidence RCS reduction versus frequency due to the one dimensional curvature of a rectangular section of a leaf with Mg = 0.7 and τ = 0.5 mm for three different radii of curvature using the numerical (9) (——) and analytical (15) (---) expressions.

Figure A-1: Geometry for the scattering of a plane wave by a tilted resistive sheet.

References

1. LeVine, D. M., A. Schneider, R. H. Lang, and H. G. Carter, "Scattering from thin dielectric disks," IEEE Trans. Antennas Propagat. Vol. AP-33, No. 12, pp. 1410-1413, 1985.

2. Borel, C. C., and R. E. McIntosh, "A backscattering model for various foliated deciduous tree types at millimeter wavelengths," Proceedings of IEEE Geosci. Remote Sens. Symposium, Zurich, 8-11 Sept. 1986.

3. Senior, T. B. A., K. Sarabandi, and F. T. Ulaby, "Measuring and modeling the backscattering cross section of a leaf," Radio Sci., in press.

4. Ulaby, F. T., and M. El-Rayes, "Microwave dielectric spectrum of vegetation material," Proceedings of IEEE Geosci. Remote Sens. Symposium, Zurich, 8-11 Sept. 1986.

5. Liepa, V.V., E. F. Knott, and T.B.A. Senior, "Scattering From Two-Dimensional Bodies with Absorber Sheets," Radiation Laboratory Report No. 011769-2-T, The University of Michigan, May 1974.

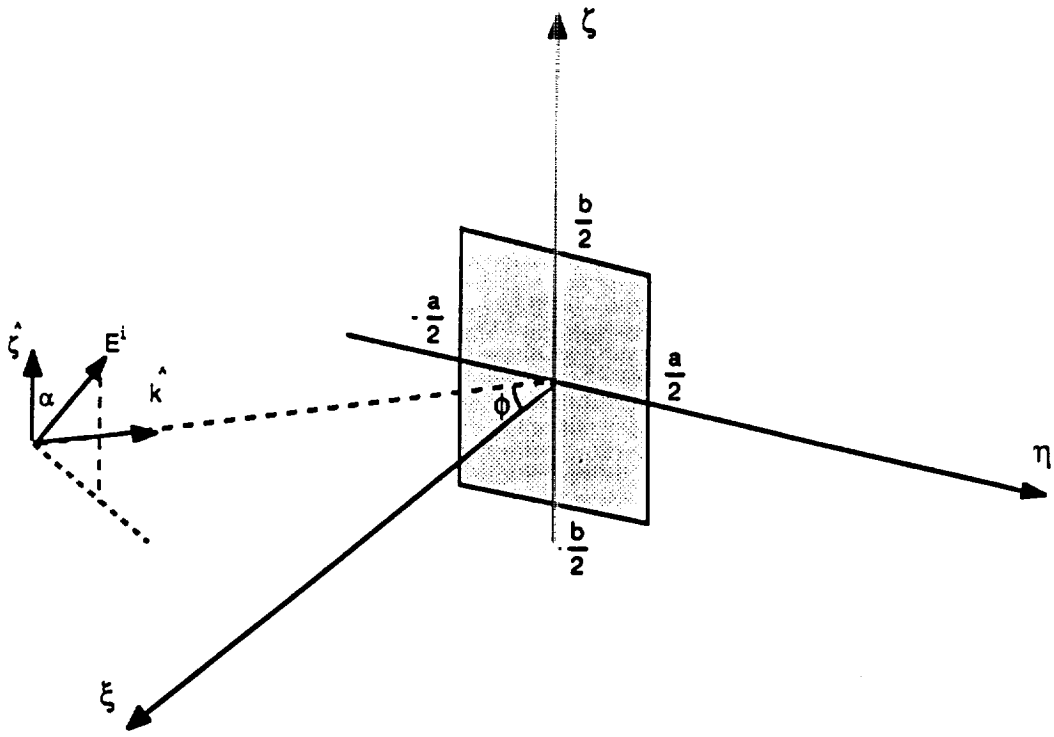
ζ
b/2
-a/2
a/2
-b/2
η
ξ
ζ
E^i
α
k
φ

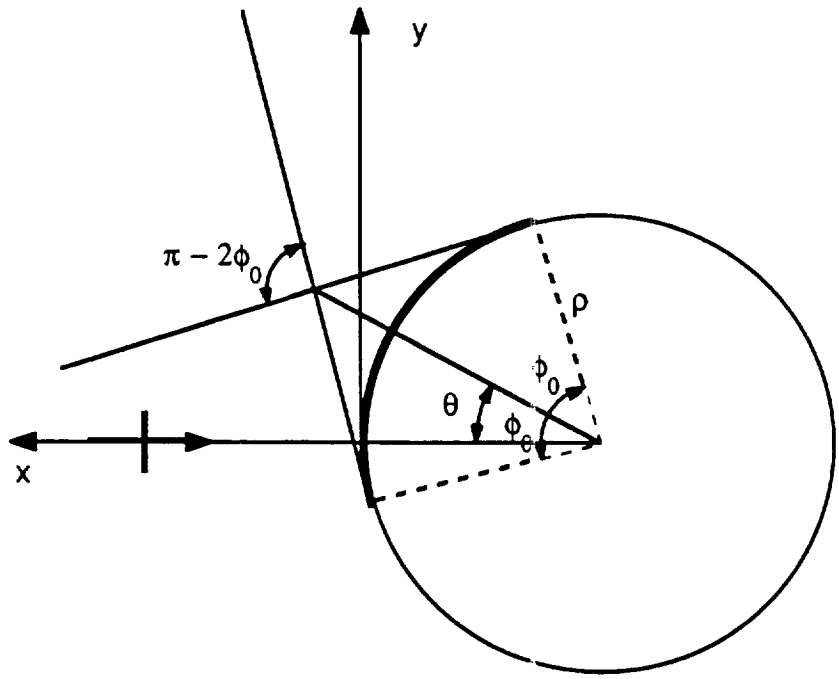
y
x
$\pi - 2\phi_0$
ρ
ϕ_0
θ
ϕ_θ

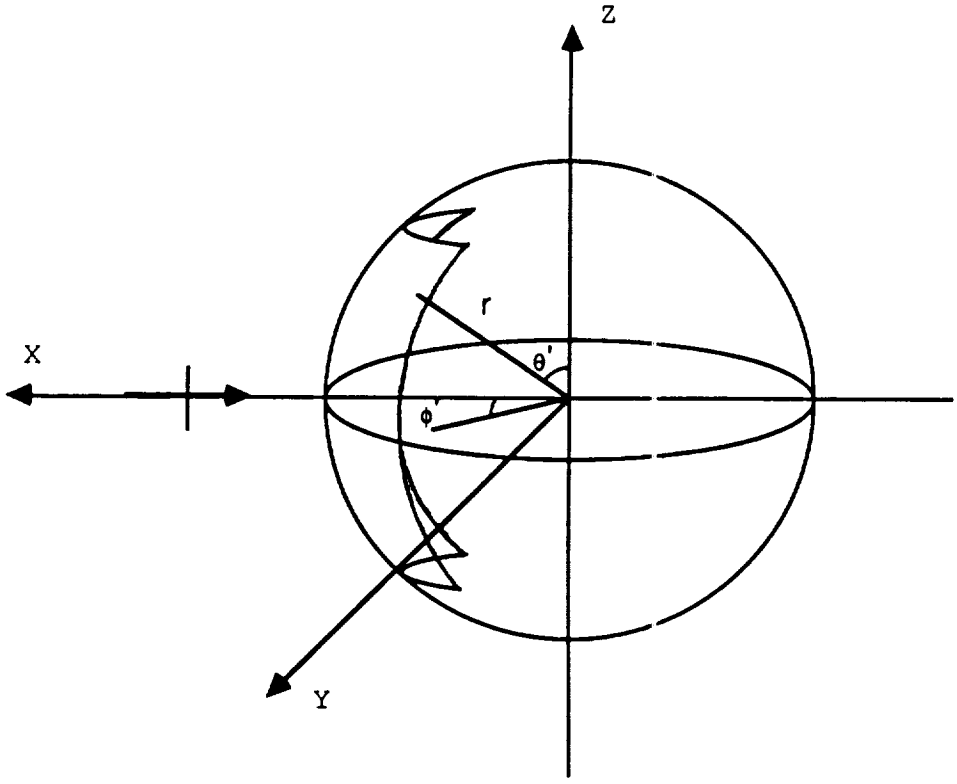
Z
X
Y
r
θ'
φ'

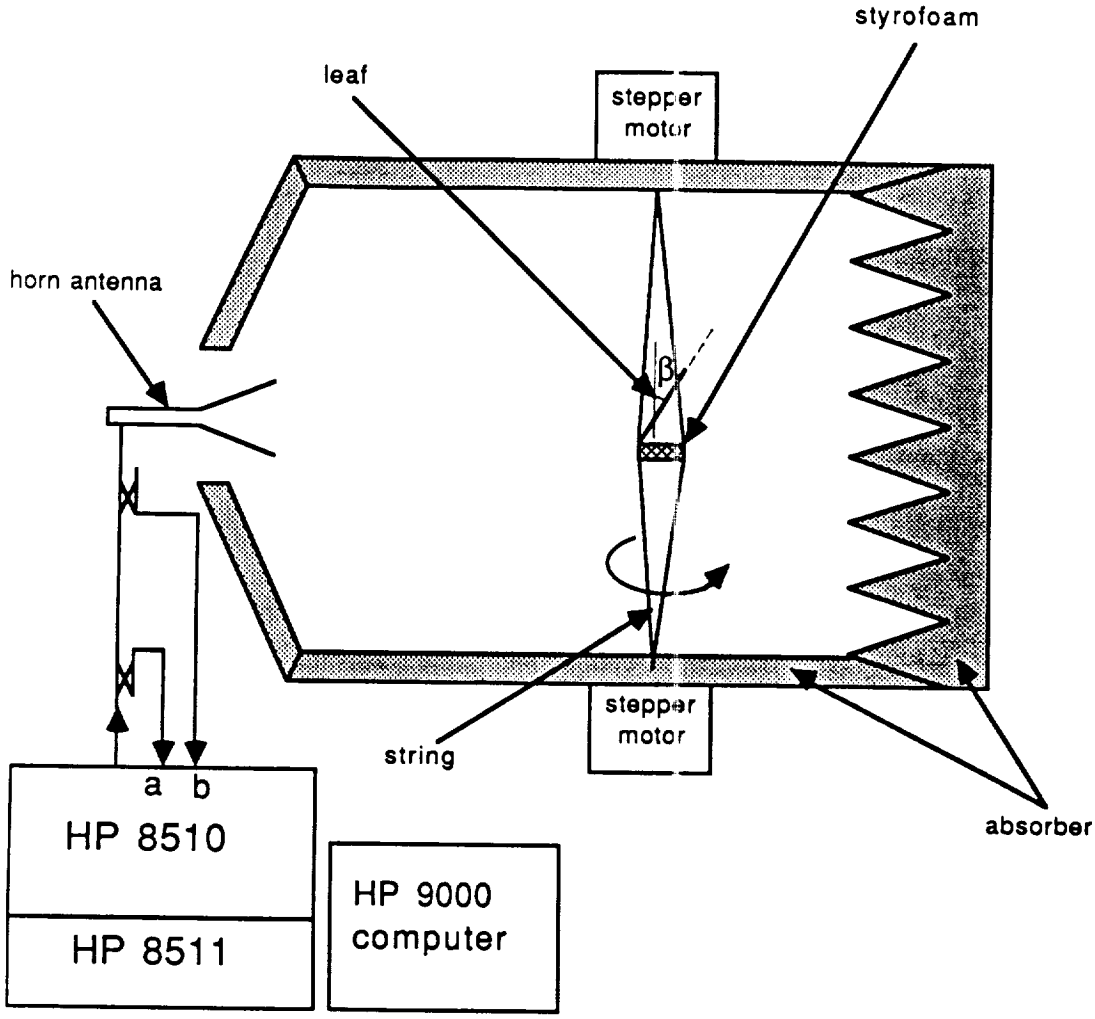
styrofoam
leaf
stepper motor
horn antenna
β
stepper motor
string
absorber
a b
HP 8510
HP 8511
HP 9000 computer

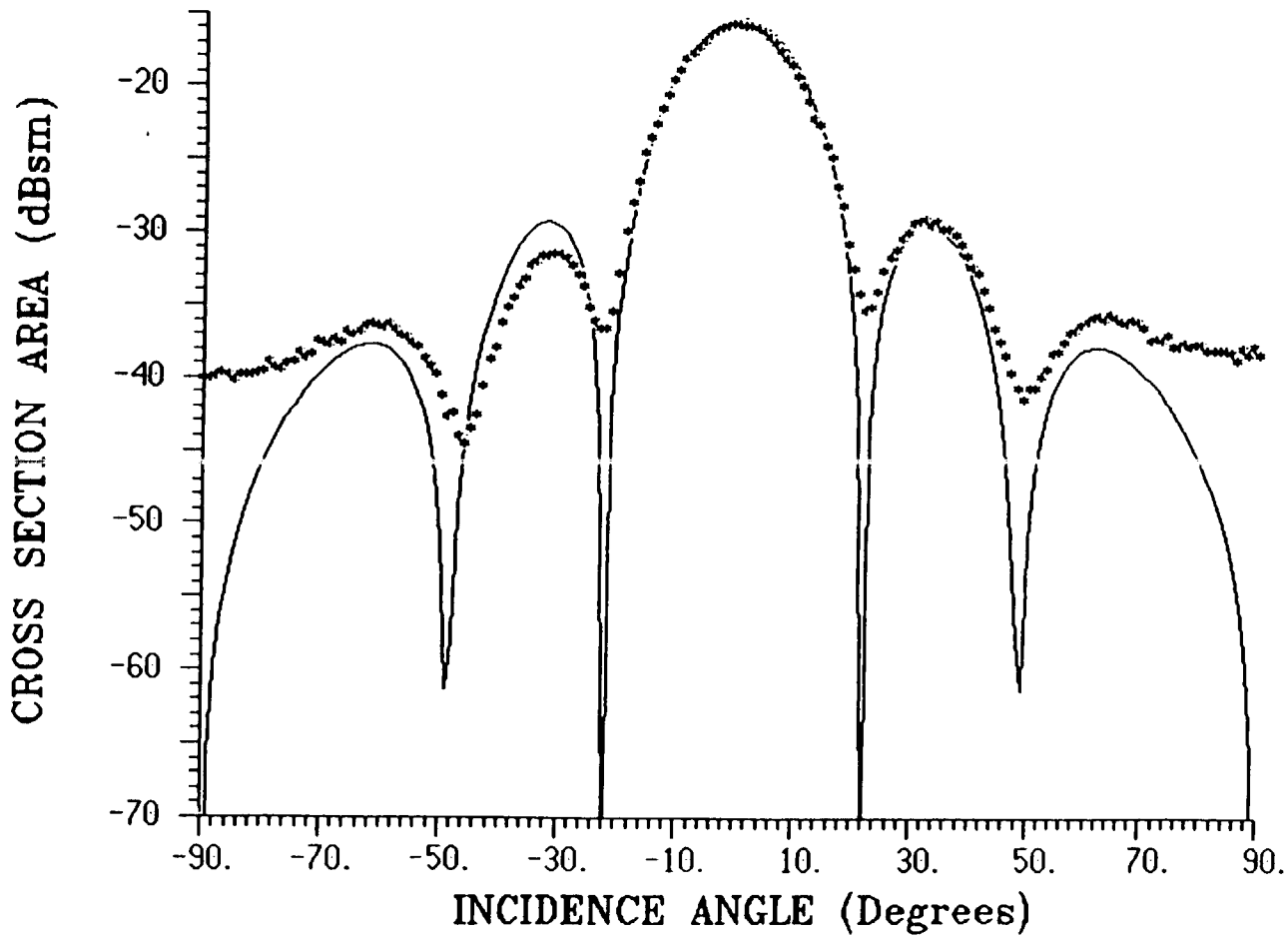
CROSS SECTION AREA (dBsm)
-20
-30
-40
-50
-60
-70
-90.
-70.
-50.
-30.
-10.
10.
30.
50.
70.
90.
INCIDENCE ANGLE (Degrees)

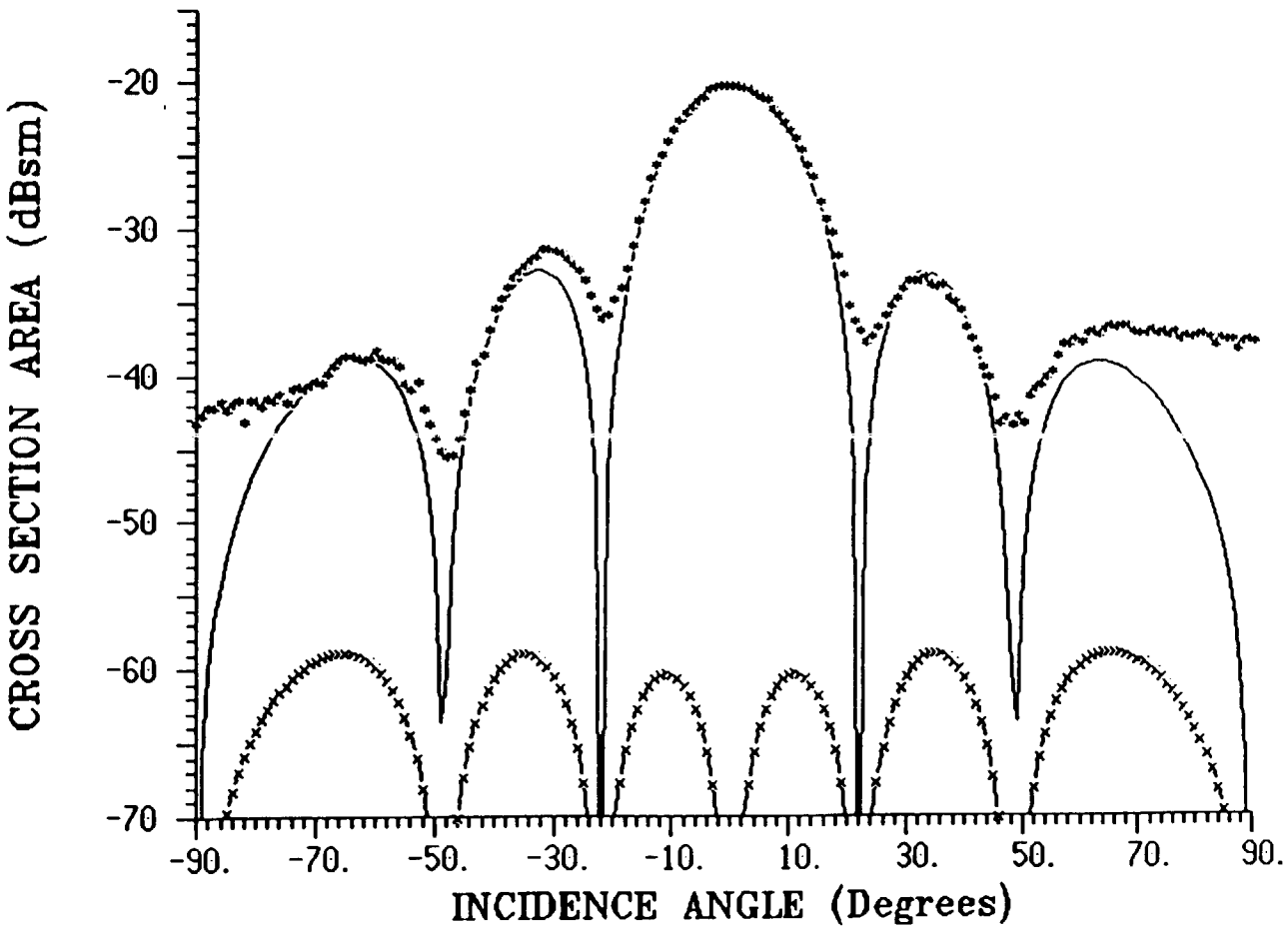
CROSS SECTION AREA (dBsm)
-20
-30
-40
-50
-60
-70
-90.
-70.
-50.
-30.
-10.
10.
30.
50.
70.
90.
INCIDENCE ANGLE (Degrees)

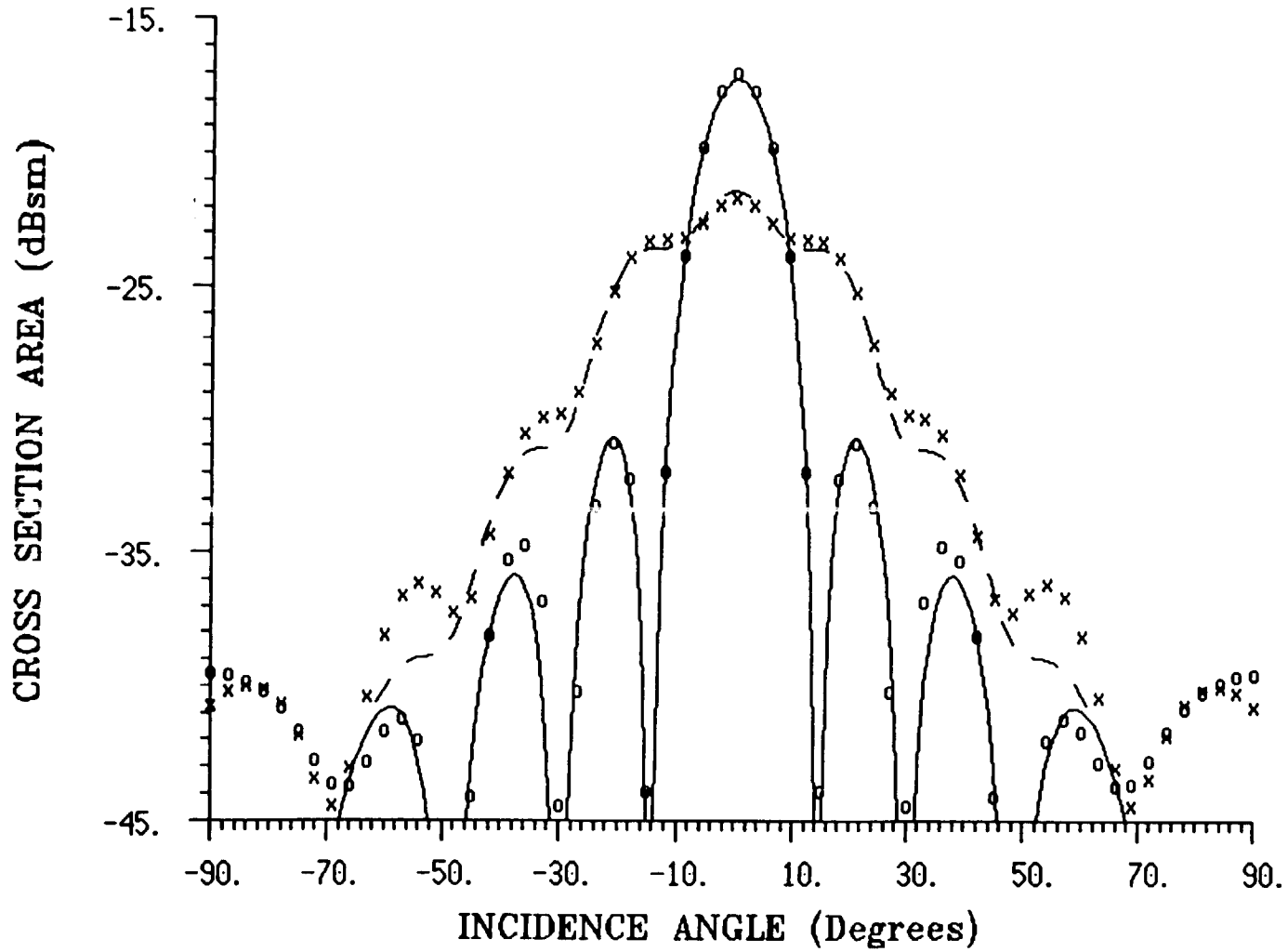
-15.
-25.
-35.
-45.
CROSS SECTION AREA (dBsm)
-90.
-70.
-50.
-30.
-10.
10.
30.
50.
70.
90.
INCIDENCE ANGLE (Degrees)

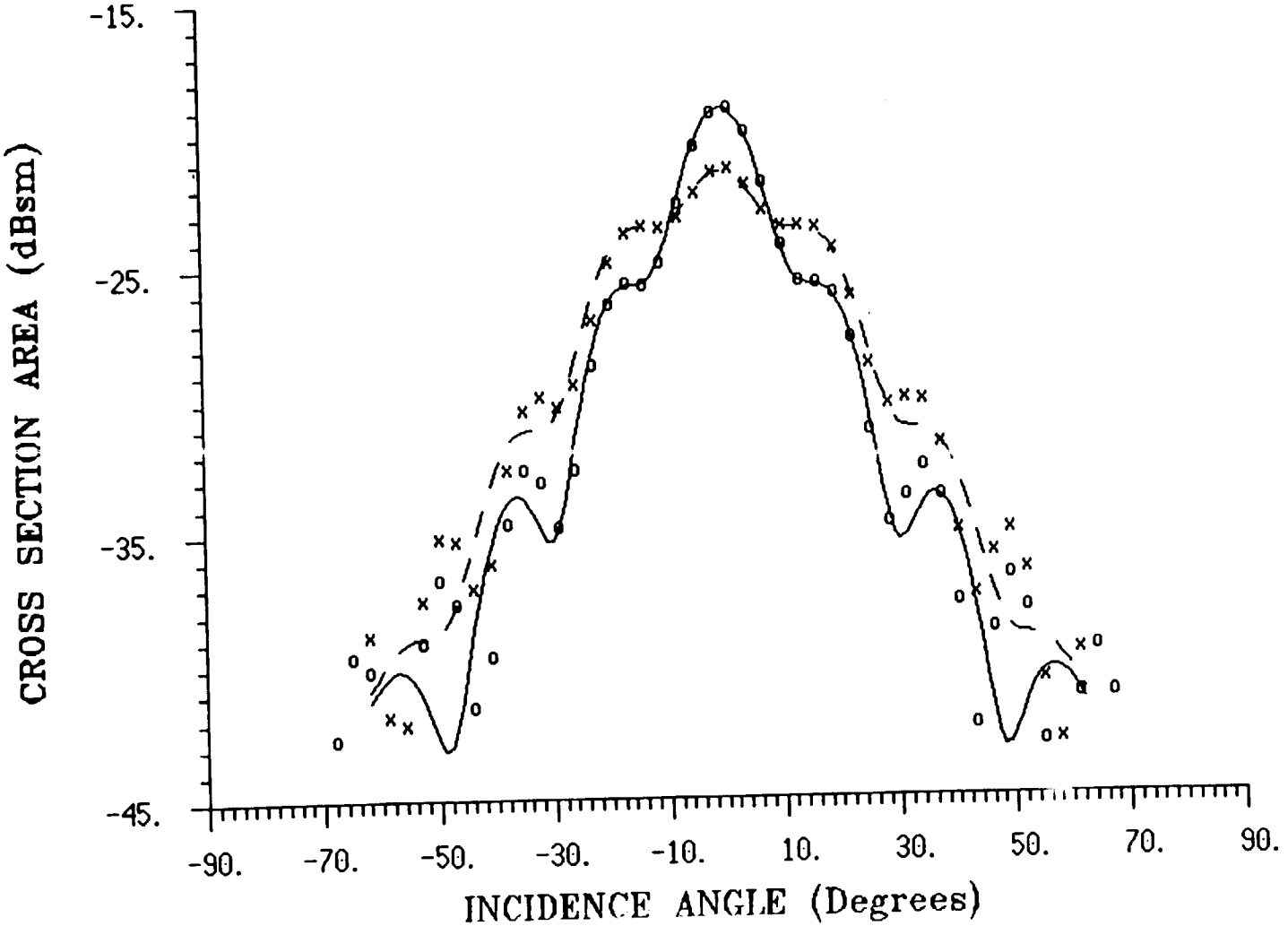
-15.
-25.
-35.
-45.
CROSS SECTION AREA (dBsm)
-90.
-70.
-50.
-30.
-10.
10.
30.
50.
70.
90.
INCIDENCE ANGLE (Degrees)

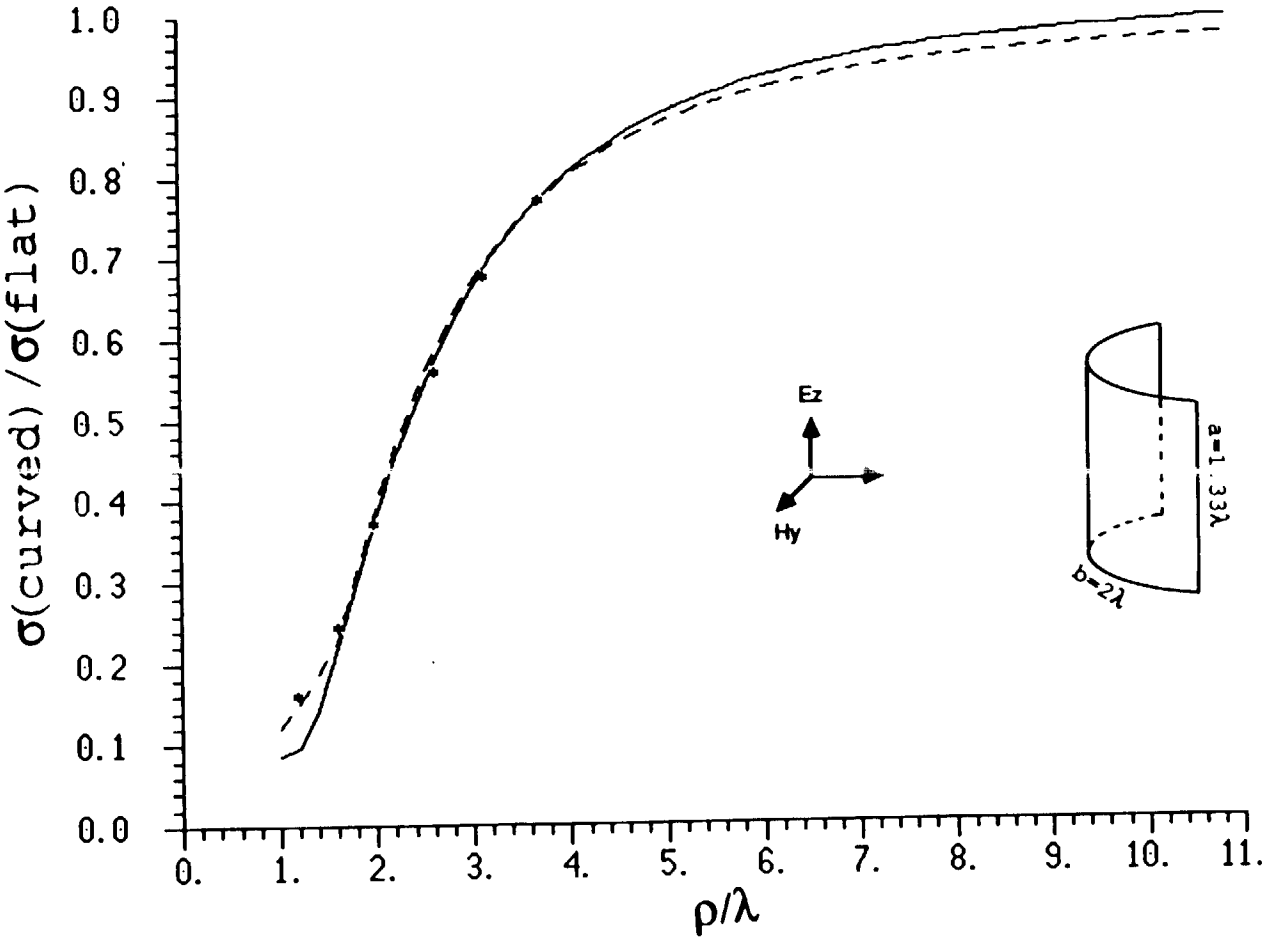
σ(curved) /σ(flat)
1.0
0.9
0.8
0.7
0.6
0.5
0.4
0.3
0.2
0.1
0.0
0.
1.
2.
3.
4.
5.
6.
7.
8.
9.
10.
11.
ρ/λ
Ez
Hy
a=1.33λ
b=2λ

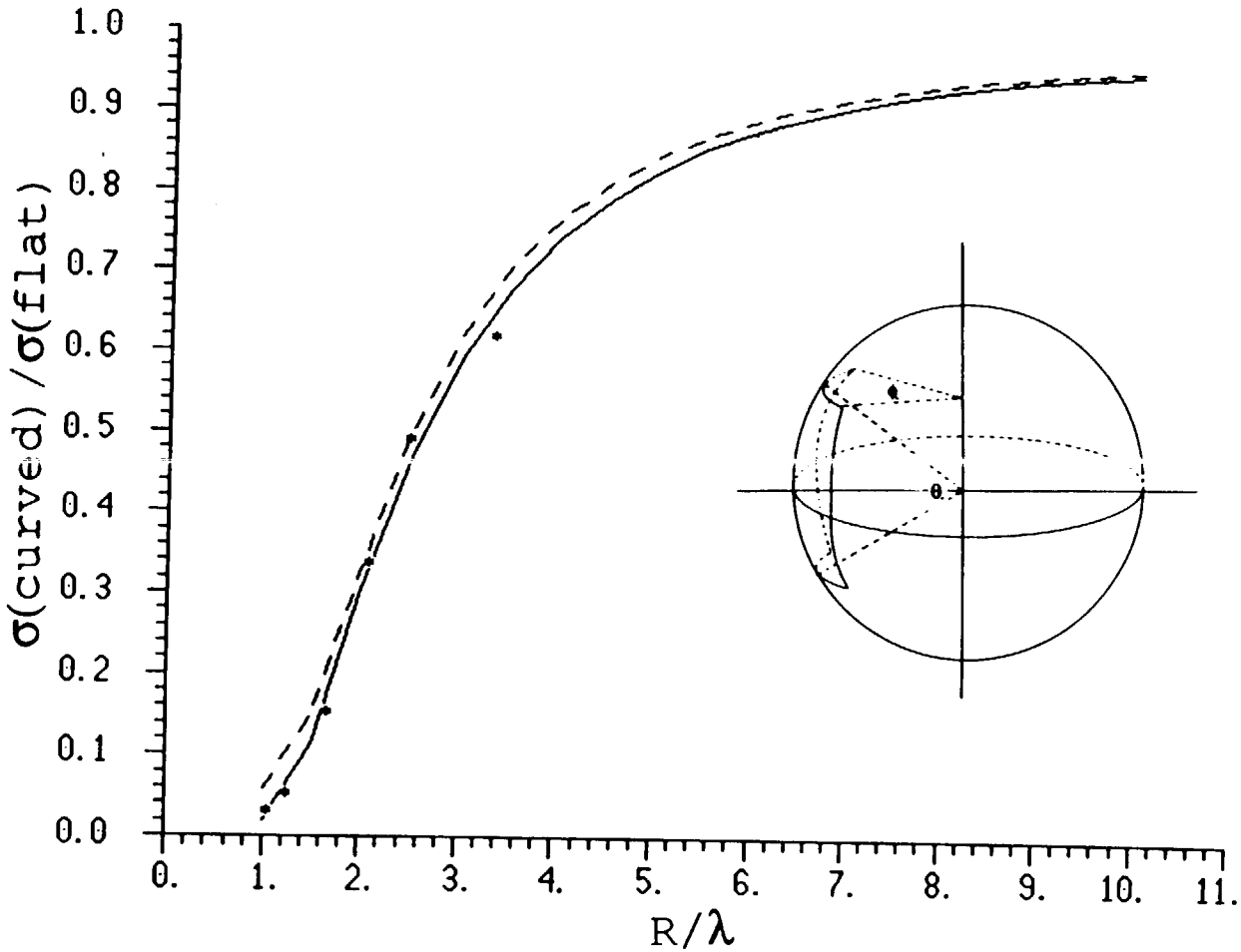
σ(curved) /σ(flat)
1.0
0.9
0.8
0.7
0.6
0.5
0.4
0.3
0.2
0.1
0.0
0.
1.
2.
3.
4.
5.
6.
7.
8.
9.
10.
11.
R/λ

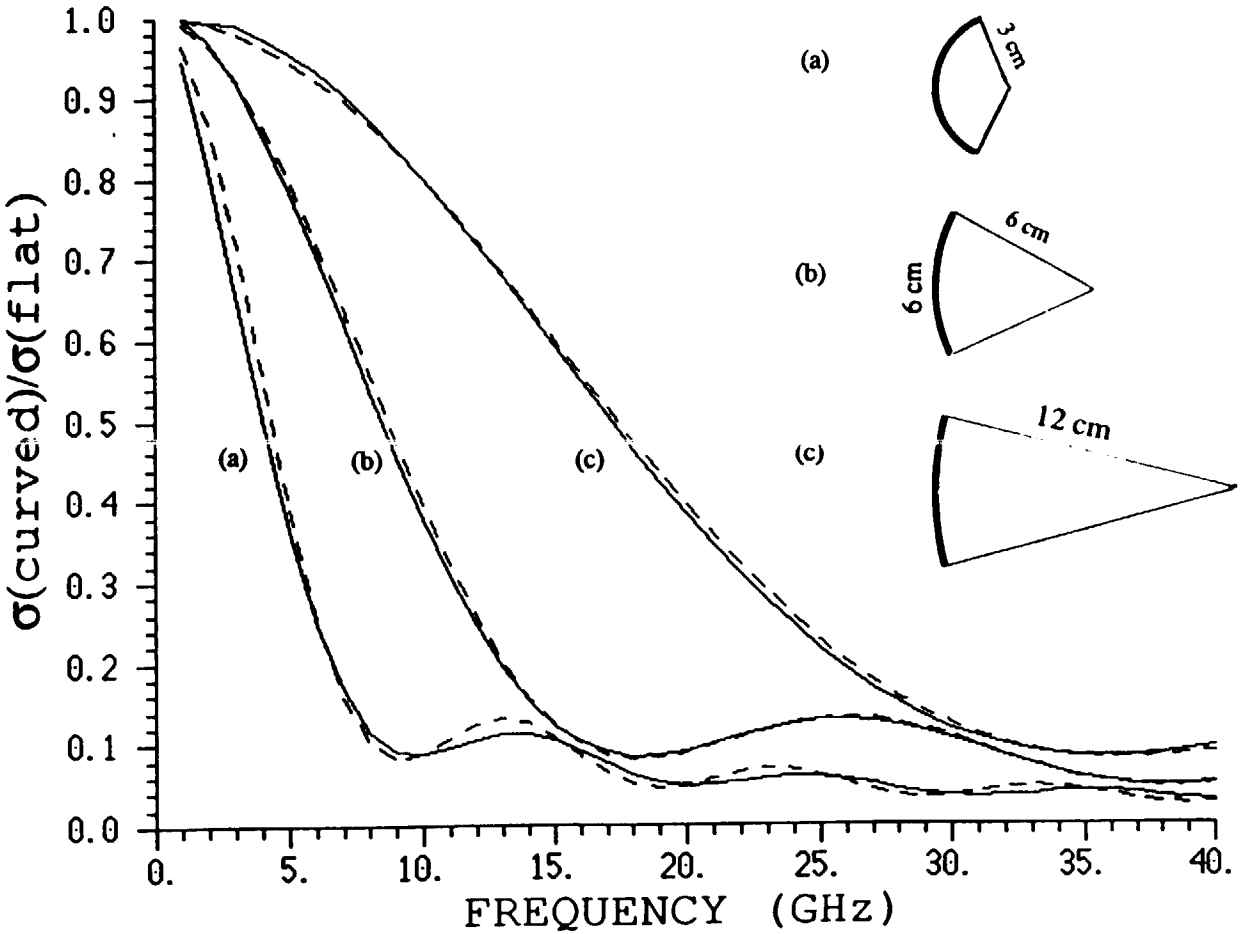
σ(curved)/σ(flat)
1.0
0.9
0.8
0.7
0.6
0.5
0.4
0.3
0.2
0.1
0.0
0.
5.
10.
15.
20.
25.
30.
35.
40.
FREQUENCY (GHz)
(a)
(b)
(c)
3 cm
6 cm
6 cm
12 cm

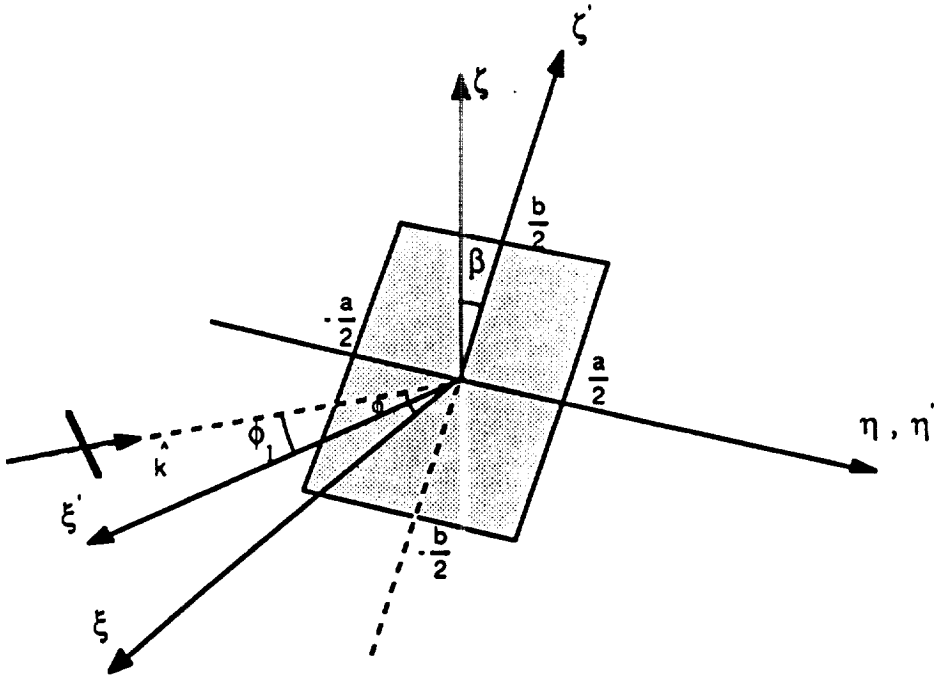
ζ'
ζ
b/2
β
-a/2
a/2
η , η'
φ
φ1
k̂
ξ'
-b/2
ξ